https://doi.org/10.48048/tis.2024.8432

Effects of pH on the Structural and Optical Properties of $CaAl_2O_4$: Eu^{2+}, Dy^{3+} Nanoparticles

Samuel Ndungu Waithira[1,*], Sharon Kiprotich[2], Ali Halake Wako[1] and George Simba Nyamato[1]

[1]*Department of Physical Sciences, University of Embu, Embu, Kenya*
[2]*Department of Physical and Biological Sciences, Murang'a University of Technology, Muranga, Kenya*

([*]Corresponding author's e-mail: samuelndunguwaithira@gmail.com)

Received: 14 May 2024, Revised: 28 June 2024, Accepted: 14 July 2024, Published: 10 October 2024

Abstract

Calcium aluminate phosphor nanomaterials co-doped with europium and dysprosium, ($CaAl_2O_4$: Eu^{2+}, Dy^{3+}) were prepared using a facile solution combustion technique. The structural and optical properties were investigated. The X-ray diffraction (XRD) results confirmed the presence of the monoclinic phase in all the samples. The Fourier-transform infrared analysis gave the expected chemical combustion results of the final product with few traces of $Ca_3Al_2O_6$ impurities at low and very high Potential of Hydrogen (pH). The XRD patterns showed the presence of an impurity phase at low pH. This impurity phase was caused by preferential precipitation in the starting mixture due to a lack of homogeneity in the precursor mixture between the urea and metallic ions hence poor combustion. The diffraction angles of the major peaks shifted to lower 2θ for all the samples except for the sample synthesized at pH = 3.4 which shifted to higher 2θ. The crystallite sizes of the as-prepared samples were determined using the Debye-Scherrer equation. It was noted that there was variation in the crystallite sizes with a change in pH. The effect of pH was also observed in the Ultraviolet-Visible (UV-Vis) studies. It was also noted that the band gap increased with an increase in pH from 2.9 to 4.5. Scanning electron microscope (SEM) micrographs showed that all samples were agglomerated and had irregular shapes with pores and cracks. The study provides a simple route to synthesize $CaAl_2O_4$: Eu^{2+}, Dy^{3+} phosphors with the optimum synthesis pH producing the most crystalline sample for application in lighting devices.

Keywords: $CaAl_2O_4$: Eu^{2+}, Dy^{3+}, Phosphors, Nanomaterial, pH, Combustion synthesis

Introduction

Phosphors are solid-state materials that exhibit the phenomenon of luminescence, whereby they emit light upon excitation. These materials can exist as finely divided powders or as thin films. Luminescence occurs when phosphors absorb energy in the form of ultraviolet (UV) radiation, visible light or thermal radiation, subsequently re-emitting this energy within the visible spectrum [1]. The luminescent properties of phosphors are governed by their composition, which typically includes a host lattice doped with specific activator ions. The host lattice is often composed of alkaline earth metal aluminates such as calcium aluminate ($CaAl_2O_4$), barium aluminate ($BaAl_2O_4$) and strontium aluminate ($SrAl_2O_4$) [2]. The activator ions, which are responsible for the luminescence, are commonly rare earth elements, including europium (Eu), dysprosium (Dy) and neodymium (Nd). These dopants introduce

electronic energy levels within the bandgap of the host lattice, facilitating the absorption and subsequent emission of light. Phosphors are crucial in technology and industry due to their luminescent properties, converting energy into visible light. Their emission wavelengths can be tailored, ensuring optimal visibility. Phosphors exhibit high durability and stability against environmental factors, maintaining performance in various conditions. Additionally, their versatility allows integration into different materials [3]. They are essential in display screens, LEDs, and fluorescent lamps, enhancing visual technology and lighting efficiency. In medical imaging and radiation detection, phosphors enable precise diagnostics by emitting light in response to X-rays or radiation [4]. Additionally, they play a vital role in security, environmental monitoring, and scientific research through their ability to detect and measure various phenomena. In recent years, researchers have focused on phosphors because of their suitability in many industrial applications including emergency guidance during intentional blackouts, in light emitting devices, fluorescence lamps, watches, demarcation of loads and radiation dosimeter [5,6]. pH optimization enhances their performance by improving crystallinity and phase purity, leading to higher luminescence efficiency and controlling particle size and morphology for consistent optical properties.

Intense broad-band emission from the deep blue to red region of the electromagnetic spectrum is typically displayed by phosphors doped with Eu^{2+} and Dy^{3+} [7]. The allowed transition between the $4d^6 5f^1$ excited state to $4d^7$ ground state of Eu^{2+} is responsible for the luminescent emission observed. Eu^{2+} forms shallow trap below the conduction band and when electrons are excited, they are promoted to the conduction band then trapped in the shallow traps [8]. Adding Dy^{3+} as a co-dopant, will lead to formation of intermediate traps and deeper traps which can capture more electrons and hence leading to longer afterglow of the phosphor [9]. $CaAl_2O_4$ is said to have a dominant hexagonal structure that remains unchanged even after doping from rare earth metal/lanthanide, Europium ion (Eu^{2+})[10]. The long-time used Sulphide phosphors are inferior to aluminate (Al_2O_4) phosphors doped with Eu^{2+} dopant [11]. Zinc Sulphides phosphors (ZnS; Cu) have been used as luminescent materials but due to their very short decay time, they are doped with radioactive isotopes to improve luminescence, which makes them harmful. This made the use of this type of phosphor prohibited hence there was a need to replace them [12]. The dopant emits a broadband spectrum since the dopant undergoes electron transition from $4f^6\ 5d^1$ to $4f^7$. This is because the excited Eu^{2+} ion is very unstable in a changed lattice structure [11].

Alkaline-earth aluminate phosphors exhibit long photoluminescence intensity for a long period and are chemically stable [13], hence our interest in $CaAl_2O_4$:Eu^{2+} phosphor. It emits maximum spectra, blue in color, at 490 - 495 nm as Eu^{2+} undergoes electron transition. However, co-doping done using other ions of the rare earth metal group leads to emission spectra within the green region at a maximum wavelength of 500 nm [14]. The co-doping of $CaAl_2O_4$: Eu^{2+} phosphor with other ions of the rare earth metal group generates deeper traps, hence longer afterglow phosphorescence [14].

Researchers have come up with many methods for the synthesis of phosphor materials. These methods include microwave-assisted chemical precipitation method for the synthesis of $CaAl_2O_4$: Eu^{2+}, Nd^{3+} [15], Sol-gel method which was adopted in the synthesis of Ba_2SiO_4: Sm^{3+} [16], hydrothermal synthesis method used in the synthesis of $Bi_4Ge_3O_{12}$: Eu^{3+} phosphors [17] and solid -Sate reaction method [18]. In this study, the solution combustion technique was utilized as the method of choice for the synthesis of $CaAl_2O_4$: Eu^{2+}, Dy^{3+}. Compared to other methods, the combustion method helps to control the amount of each component, gives a uniform mixture, needs low synthesis temperature and takes a short time [11].

The host matrix and synthesis conditions affect the structural and optical properties of phosphors. pH significantly affects the structural properties of $CaAl_2O_4$: Eu^{2+}, Dy^{3+}nanoparticles by influencing crystallinity, particle size and morphology through its control of nucleation and growth processes. pH

affects the preferential precipitation of the phosphor at low pH for example, there is no complete combustion, and hence the Ca and Al will not be completely precipitated giving rise to poorly developed crystal impurity alongside the pure crystal. In a research done by Shafia *et al.* [19], on $SrAl_2O_4$: Eu^{2+}, Dy^{3+} phosphor, it was noted that at pH around the 3 - 5, there was complete combustion and pure crystal was formed. At very high pH, there was preferential precipitation of aluminum oxohydroxide in the precursors solution owing to the formation of impurities. It is worth noting that at neutral pH aluminum trihydroxide (Al $(OH)_3$ starts to precipitate and at certain conditions, water molecule was also lost from aliminium trihyroxide forming AlO(OH) leading to poor homogeneity and formation of suitable complex at high pH. The luminescence properties of phosphors are greatly influenced by pH. pH significantly impacts the optical properties of $CaAl_2O_4$: Eu^{2+}, Dy^{3+}nanoparticles by affecting defect concentration, which influences luminescence efficiency, and altering the local environment of dopant ions, modifying emission intensity and wavelength. The excitation intensity slowly increases with an increase in pH [20]. pH variation to a great extent affects the morphology of the sample which in turn affects the luminescence properties hence affecting the application suitability in different fields [21]. Although the phosphorescence of $CaAl_2O_4$: Eu^{2+} is known, information about the effect of different dopants and other synthesis conditions is paucity of information. This study seeks to investigate the influence of pH on the structure and optical properties of $CaAl_2O_4$: Eu^{2+}, Dy^{3+} nanoparticles. Investigating the effects of pH on the structural and optical properties of $CaAl_2O_4$: Eu^{2+}, Dy^{3+} nanoparticles is of significant novelty and importance. Understanding pH's impact on these nanoparticles can lead to optimized synthesis conditions, enhancing their luminescent efficiency and stability. This research can reveal crucial insights into the tunability of their properties for various applications, such as advanced lighting, display technologies and bio-imaging. By exploring this relationship, we can potentially develop superior phosphor materials with tailored characteristics for specific industrial and technological needs.

Experimental procedure

Eu^{2+} doped and Dy^{3+} co-doped, calcium aluminate phosphor was synthesized using the combustion method with slight modification[23-26]. The starting materials consisted of the analytical pure grade of $Al(NO_2)_2{\cdot}9H_2O$, $Ca(NO_2)_2$, $Dy(NO_3)_3$, $Eu(NO_3)_3{\cdot}5H_2O$ and urea ($CO(NH_2)_2$) as the fuel all obtained from MERCK in analytical purity of 99.9 % and used as received. The precursors were prepared with ratios of $Ca(NO_2)_2$ and $Al(NO_2)_2{\cdot}9H_2O$ kept constant at 1:2 mol%. The doping concentrations of Eu^{2+} and Dy^{3+} were also kept constant at 0.2 mol%. To investigate the effects of pH, ammonium carbonate $(NH_4)_2CO_3$ was added in different amounts to vary the pH of the solution.

Five samples were prepared with pH of 2.9, 3.0, 3.4, 3.9 and 4.5. The doping concentrations of both Eu^{2+}, Dy^{3+} was also kept constant at optimum concentration and synthesized at a constant muffle furnace temperature of 500 °C. Using a magnetic stirrer, the precursors were mixed for 15 min at room temperature to obtain a homogeneous solution. The solution was then poured into crucibles and placed in a muffle furnace preheated at 500 °C. The solution boiled then evaporated, and decomposed with the release of gases (oxides of nitrogen, carbon and ammonia) smoke and fumes. Spontaneous ignition then occurred followed by combustion with vast swelling and white foam was produced. The foam produced was cooled to room temperature and milled to form the final product.

To study the effects of pH on the structural and optical properties of $CaAl_2O_4$: Eu^{2+}, Dy^{3+} nanoparticles, several experimental techniques are essential. The samples were further characterized using various analytical techniques. JEOL JSM-7500F field emission scanning electron microscope (FE-SEM) was used to investigate the product particles' morphologies. Perkin-Elmer Lambda 750S UV-Vis spectrometer was used to record the UV-Vis absorption spectra of the phosphor material. The crystallinity and phase of the samples were investigated using an X'Pert PRO PANalytical XRD diffractometer with CuKα at λ = 0.15405 nm to obtain the samples' X-ray diffraction (XRD) patterns. The consistency of the

sample components and the type of bonds present was investigated using an FT-IR360 infrared spectrometer using KBr pellets in the region of 4,000 - 400 cm^{-1}.

Results and discussion

Fourier Transform Infra-Red (FTIR) analysis

Figures 1(a) - 1(d) shows the FTIR patterns of $CaAl_2O_4$: Eu^{2+}, Dy^{3+} synthesized at pH of 2.9, 3.0, 3.9 and 4.5, respectively. In the region 462 to 579 cm^{-1}, traces of $Ca_3Al_2O_6$ phase are detected [27]. From **Figure 1**, a strong band at 1,428.79 cm^{-1} for pH = 2.9 in **Figure 1(a)**, 1,432.58 cm^{-1} for pH = 3.0, in **Figure 1(b)**, 1,430.09 cm^{-1} for pH = 3.9 in **Figure 1(c)** and 1,421.65 cm^{-1} for pH = 4.5 in **Figure 1(d)**. These bands are attributed to nitrate (NO_3^-) vibrations usually observed between 1,250 to 1,650 cm^{-1} [28]. The stretching vibration of AlO_4 is observed at 827.69, 810.17, 818.23 and 781.81 cm^{-1} for pH 2.9 in **Figure 1(a)**, 3.0 in **Figure 1(b)**, 3.9 in **Figure 1(c)** and 4.5 in **Figure 1(d)**, respectively while the stretching vibrations of the metal oxides of Al-O, Ca-O and Ca-O-Al bonds are seen at 573.63 cm^{-1} for pH = 2.9 in **Figure 1(a)**, 579.09 cm^{-1} for pH = 3.0 in **Figure 1(b)**, 462.66 and 571.18 cm^{-1} for pH = 3.9 in **Figure 1** and 571.76 cm^{-1} for pH = 4.5. The absorption bands of AlO_4 are seen in the region between 680 - 500 cm^{-1} [29]. Absorption bands of 3,704.39 cm^{-1} (**Figure 1(c)**) and 3,679.44 cm^{-1} (**Figure 1(d)**) are associated with symmetric stretching vibration of water vapor absorbed by the samples from the atmosphere.

X-Ray Diffraction (XRD) analysis

To get information about the crystal structure of as-prepared $CaAl_2O_4$: Eu^{2+}, Dy^{3+}, x-ray diffraction (XRD) measurements were determined. The XRD patterns of $CaAl_2O_4$: Eu^{2+}, Dy^{3+} synthesized at pH of 2.9, 3.0, 3.4, 3.9 and 4.5 are shown in **Figure 2**. The powders' XRD patterns are dominated by the monoclinic phase diffraction peaks of $CaAl_2O_4$ and all the peaks can be indexed to the typical monoclinic $CaAl_2O_4$ phase matching with the ICDD data file no. 069 - 0033 for orthorhombic structure.

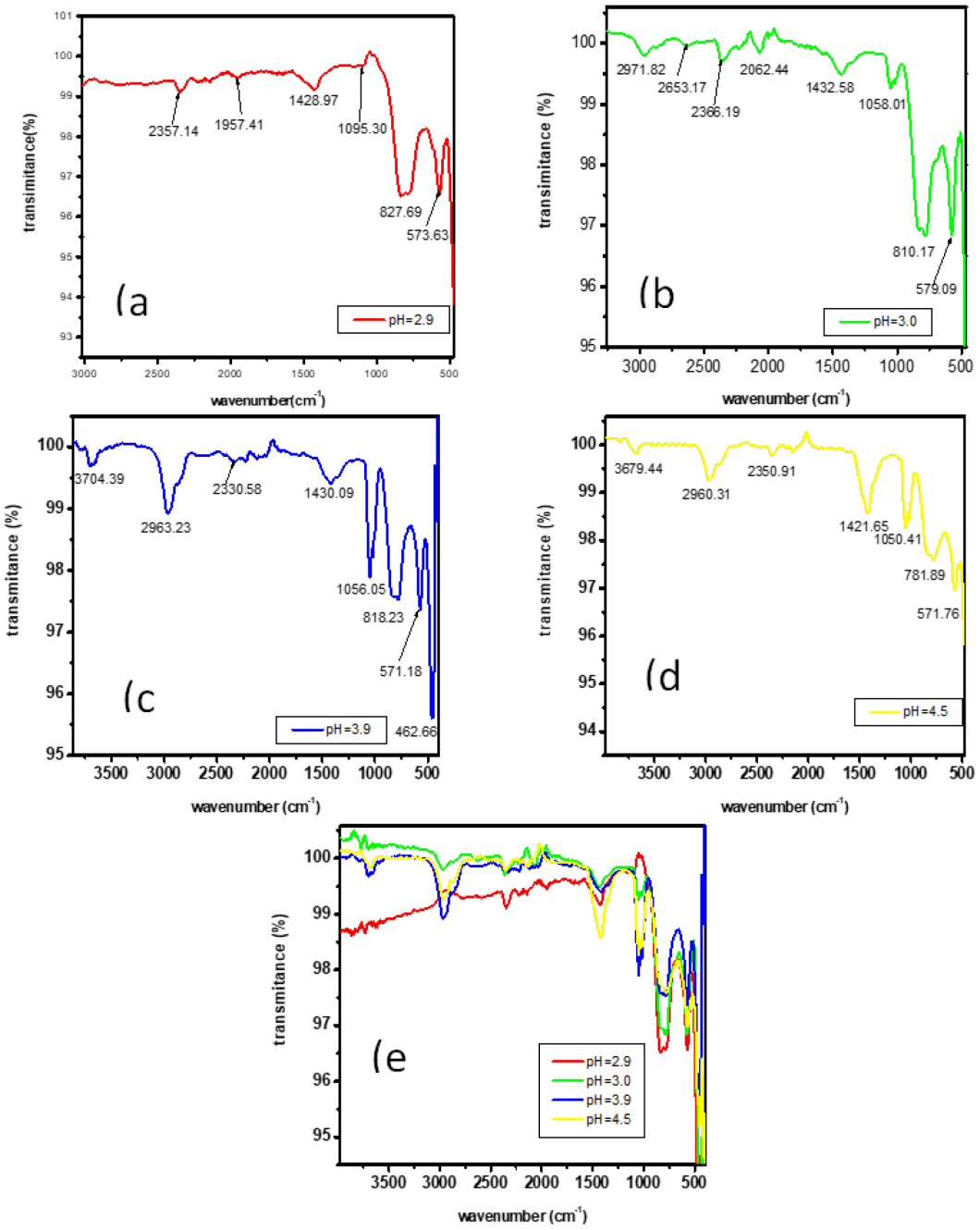

Figure 1 FTIR spectra of $CaAl_2O_4$: Eu^{2+}, Dy^{3+} synthesized at pH of (a) 2.9, (b)3.0, (c)3.9, (d) 4.5 and (e) for combined.

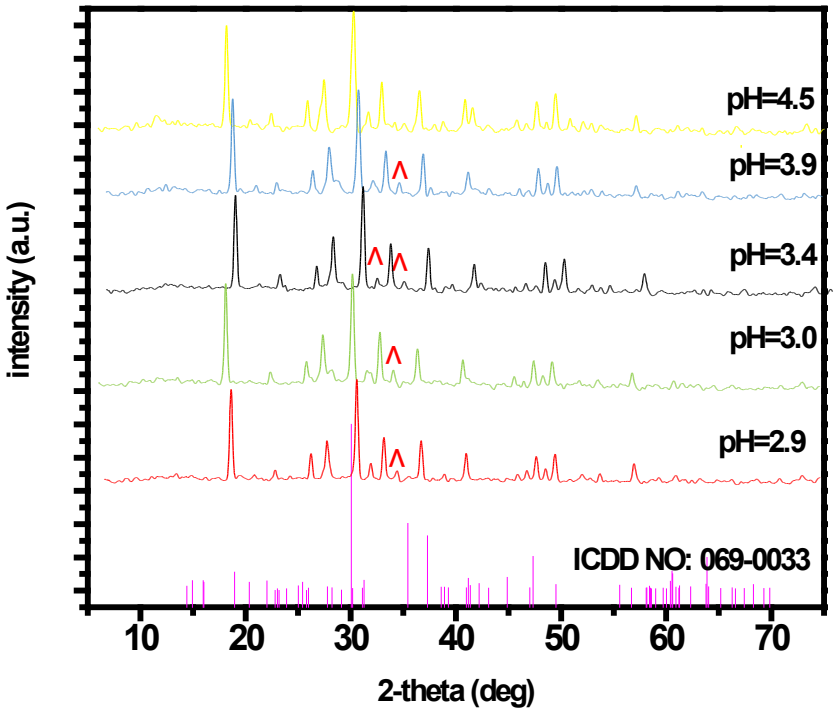

Figure 2 XRD patterns for $CaAl_2O_4$: Eu^{2+}, Dy^{3+} phosphor synthesized at different pH values.

From **Figure 2**, the XRD patterns showed the presence of a few impurity phases (shown by red inverted v) at low pH (pH < 3.9). This impurity phase is caused by preferential precipitation in the starting mixture due to a lack of homogeneity in the precursor mixture between the urea and metallic ions hence poor combustion. A similar observation was also noted by Hsu and Lu [30] in their work on the influence of pH on the formation and luminescence properties of sol-gel derived $SrAl_2O_4$: Eu^{2+}, Dy^{3+} phosphor. They reported the presence of impurity phases in samples prepared at low pH levels (below 3), but these impurity phases diminished as the pH increased [31]. The diffraction angles of the major peaks shift to lower 2θ for all the samples except for the sample synthesized at pH = 3.4 which shifts to higher 2θ as shown in **Figure 2** and **Table 1**. Shifting the diffraction angle to a higher 2θ shows the presence of compressive stress while shifting to a lower 2θ shows the presence of tensile stress in the samples [22]. The sample synthesized at pH = 3.0 had the highest intensity of 143 cps deg. as shown in **Table 1**.

Table 1 Summary of full width at half maximum (FWHM) intensity and 2θ values of the highest diffraction peaks for $CaAl_2O_4$: Eu^{2+}, Dy^{3+} phosphor synthesized at different pH.

pH	2θ (deg)	Intensity (cps deg)	FWHM(deg)
2.9	33.686	140	0.147
3.0	33.604	143	0.18
3.4	33.811	128	0.170
3.9	33.702	130	0.276
4.5	33.701	133	0.152

The crystallite size (D) of the product obtained was determined using Debye-Scherrer's equation (Eq. (1)).

$$D = \frac{K\lambda}{\beta \cos\theta} \quad (1)$$

where D is the Crystallite size, λ is the wavelength of CuKα radiation (0.154 nm), β is the full width at half maximum (FWHM) broadening, θ is the Bragg's diffraction angle and K is shape factor (0.9) [1].

Table 2 Summary of calculated values using equation (1) for $CaAl_2O_4$: Eu^{2+}, Dy^{3+} phosphor synthesized at different pH.

pH	β (deg)	β (rad) (β×Π/180)	2θ (deg)	θ (deg)	θ (rad) (θ×Π/180)	Average (nm)
2.9	0.147	0.002565634	33.686	16.843	0.293965806	46.1313751
	0.197	0.003438299	18.431	9.2155	0.160840817	
	0.200	0.003490659	30.070	15.035	0.262410253	
3.0	0.180	0.003141593	33.604	16.802	0.293250221	40.66355469
	0.187	0.003263766	18.373	9.1865	0.160334672	
	0.250	0.004363323	30.028	15.014	0.262043734	
3.4	0.170	0.00296706	33.811	16.9055	0.295056637	50.12199899
	0.188	0.003281219	18.531	9.2655	0.161713482	
	0.140	0.002443461	30.150	15.075	0.263108385	
3.9	0.276	0.004817109	33.702	16.851	0.294105432	31.78077088
	0.231	0.004031711	18.427	9.2135	0.160805911	
	0.270	0.004712389	30.040	15.02	0.262148454	
4.5	0.421	0.007347836	33.702	16.851	0.294105432	29.58692634
	0.152	0.0026529	18.412	9.206	0.160675011	
	0.510	0.008901179	30.136	15.068	0.262986212	

The estimated crystalline size and other calculated values of most 3 intense peaks using Eq. (1) are shown in **Table 2**. The average estimated crystalline size of the obtained phosphors was, 46.13, 40.66, 50.12, 31.78 and 29.57 nm for $CaAl_2O_4$: Eu^{2+}, Dy^{3+} synthesized at pH of 2.9, 3.0, 3.4, 3.9 and 4.5, respectively. The analysis of the data reveals that the estimated crystallite size of the samples synthesized at lower pH values (specifically, pH < 3.9) is significantly larger compared to those synthesized at higher pH values (pH > 3.9). The large crystal size means that the crystal has very low strain and dissolution while the small crystal size means that the crystal has high strain and dissolution which could be attributed to preferential precipitation of starting material in the product due to poor ignition at low and high pH [32]. The sample synthesized at a pH equal to 4.5 had the smallest crystalline size and hence pH = 4.5 peaked as the best synthesis pH.

UV-Vis analysis

The optical properties of the as-prepared $CaAl_2O_4$: Eu^{2+}, Dy^{3+} synthesized at pH of 2.9, 3.9 and 4.5 were determined for the aliquots drawn from the freshly prepared sample using UV-Vis

spectrophotometer with excitation wavelengths ranging from 200 to 500 nm. The data obtained was used to plot the graphs in **Figure 3**.

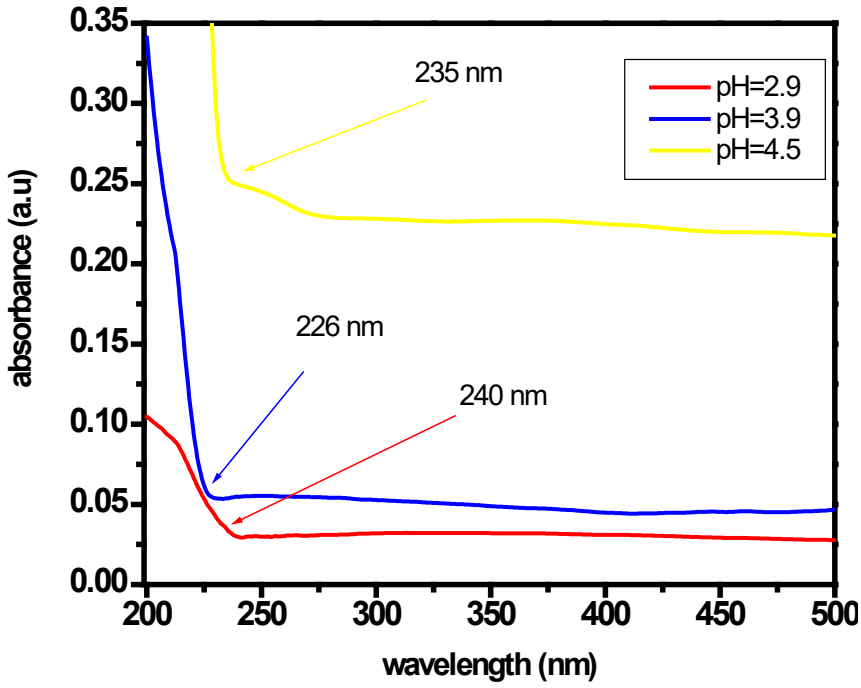

Figure 3 Absorption edges for representative samples of $CaAl_2O_4$: Eu^{2+}, Dy^{3+} phosphor synthesized at different pH values.

From the graph, it can be seen that the sharp absorption edges shift with a change in pH. From pH 2.9 to 3.9, the absorption edge shifts to a lower wavelength while the absorption edge from pH 3.9 to pH 4.5 shifts to a longer wavelength. The shifting of the absorption edge to a lower or longer wavelength may be caused by a change in pH hence slight lattice expansion ([33]). To calculate the optical band gap energy of the as-prepare $CaAl_2O_4$: Eu^{2+}, Dy^{3+} material, Tauc and Daviss-Mott relation (Eq. (2)) [34] and Tauc plot (**Figure 4**) was used.

$$(\alpha h\nu)^n = K(h\nu = Eg) \quad (2)$$

where α is absorption coefficient, hν is incident photon energy, K is energy-independent constant and Eg is the optical band gap energy of the material. In the above equation, the exponent: "n" represent the nature of the transition [35]. For direct band gap $n = 2$ and for indirect $n = \frac{1}{2}$. In the Tauc plot, the band gap energy was estimated by plotting $(\alpha h\nu)^n$ against hν. Wavelength from the UV-Vis spectroscopy was converted to energy and the absorbance coefficient (α) was calculated from absorbance data. To get $(\alpha h\nu)^n$ plotted in the y-axis, hν was taken as incident photon energy and alpha (α) calculated from absorbance data using Beer-Lambert law (Eq. (3)).

$$I = Ioe^{-\alpha\iota} \quad (3)$$

where I is the intensity of transmitted light, Io is the intensity of incident light, α is the absorbance coefficient and ι is the path length of the light in which absorbance took place. A tangent line on the curve where $\alpha = 0$ was then drawn and the point where it touches the x-axis is taken as the optical band gap of the material.

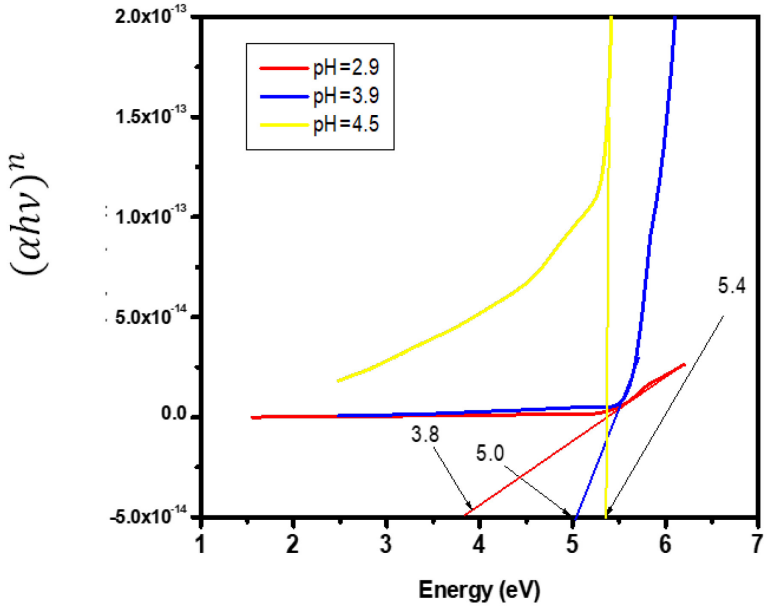

Figure 4 Tauc plot for $CaAl_2O_4$: Eu^{2+}, Dy^{3+} phosphor synthesized at different pH.

Table 3 A summary of Absorption edge and calculated values of Bandgap using Eq. (2) for $CaAl_2O_4$: Eu^{2+}, Dy^{3+} phosphor synthesized at different pH.

pH	Absorption edge (nm)	Band gap (eV)
2.9	240	3.8
3.9	226	5.0
4.5	235	5.4

From **Table 3** and **Figure 4**, it is noted that the band gap increases with the increase in pH from pH = 2.9 (3.8) to pH = 4.5 (5.4). The increase in the band gap shows that there is less delocalization and defects in the samples' structural system [36]. The sample synthesized at pH = 3.9 had a band gap of 5.0 (bulk band gap). Similar observations were reported by Kumar *et al.* [37] in their work on the adsorption of hazardous methylene blue from an aqueous solution using combustion-derived $CaAl_2O_4$: Eu^{2+} [37]. It should be noted that the band gap of the sample synthesized at pH = 4.5 had the largest band gap of 5.4 and hence admirable.

Scanning electron microscope analysis

The SEM images of the as-synthesized $CaAl_2O_4$: Eu^{2+}, $Dy^{3+}$are shown in **Figure 5**. **Figure 5(a)** shows the SEM image for $CaAl_2O_4$: Eu^{2+}, Dy^{3+} phosphor synthesized at pH = 4.5 while **Figure 5(b)** shows the SEM image for $CaAl_2O_4$: Eu^{2+}, Dy^{3+} phosphor synthesized at pH = 3.9. The SEM micrographs

(**Figure 5**) showed that the sample synthesized at pH = 4.5 has a much smaller particle size, is less agglomerated, and has more cracks and poles compared to the sample synthesized at pH = 3.9.

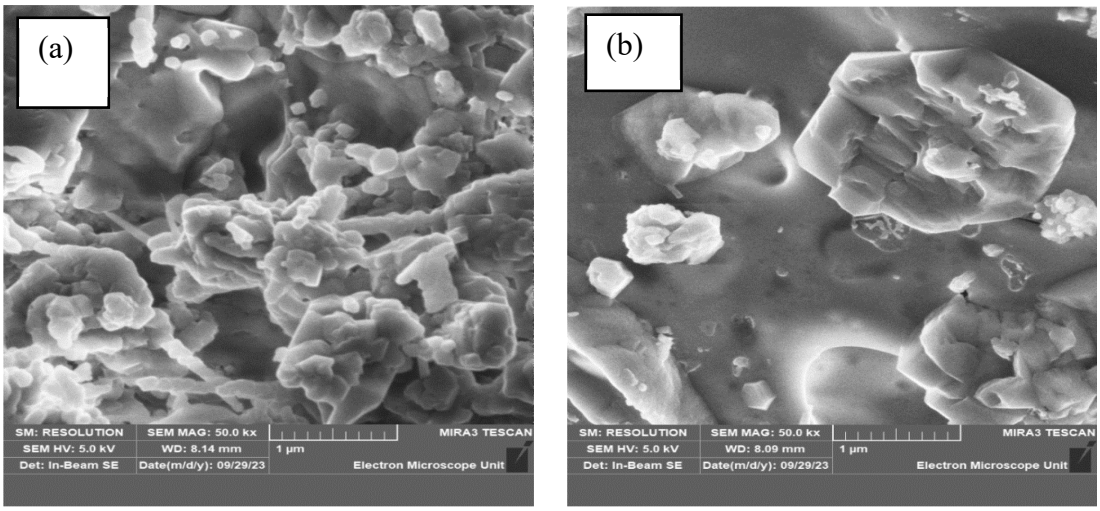

Figure 5 Representative SEM images for $CaAl_2O_4$: Eu^{2+}, Dy^{3+} phosphor synthesized at (a) pH = 4.5 and (b) pH = 3.9.

The micrographs also show that the particle shape changed from hexagonal-like to flower like with increase in pH. This observation can be attributed to an increase in crystallinity while pH is increased. The cracks and poles may be caused by the escaping gases during combustion which help in the formation of nano-crystallite material as the sintering of the phosphor is avoided as a result of the dispersion of heat by escaping gases [38]. More cracks and poles are seen in the phosphor synthesized at pH = 4.5 indicating that there was complete combustion due to a high degree of ignition in the muffle furnace leading to more exothermic reaction causing high temperature and more volume of produced gases. The agglomerates have non-uniform sizes and shapes due to irregular mass flow and non-uniform distribution of temperature during synthesis. This confirmed that the sample synthesized at pH = 4.5 obtained better combustion than that synthesized at pH = 3.9 and hence better morphology.

Figure 6 shows the EDS results and a point spectrum for $CaAl_2O_4$: Eu^{2+}, Dy^{3+} phosphor synthesized at pH = 4.5. The EDS results shown in **Figure 6** indicate that the elements of the phosphor for all samples are components of O, Al and Ca indicating that the phase of the final product was made of calcium aluminate.

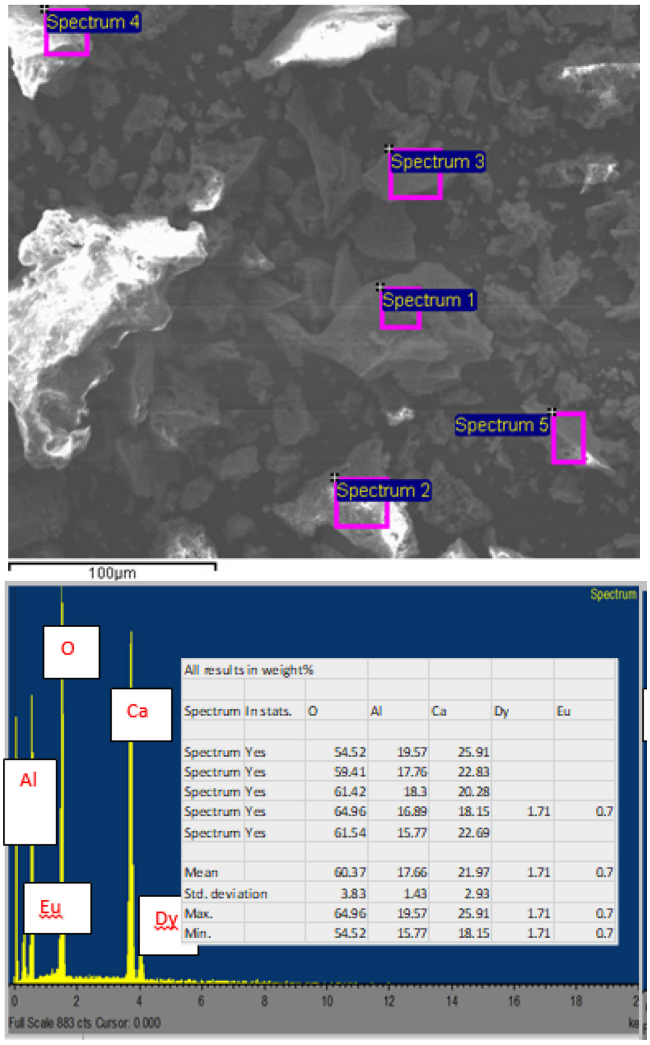

Figure 6 Representative EDS results from a point spectrum for $CaAl_2O_4$: Eu^{2+}, Dy^{3+} phosphor synthesized at pH = 4.5.

Photoluminescence of $CaAl_2O_4$: Eu^{2+}, Dy^{3+} phosphors

To enhance the photoluminescence (PL) properties, and long afterglow of $CaAl_2O_4$, Eu^{2+} and Dy^{3+} ions are used [39]. To explain the cause of these properties, trap and hole mechanisms have been adopted. In the trap mechanism, the allowed transition between the $4f^65d^1$ excited state to $4f^7$ ground state of Eu^{2+} is responsible for the luminescent emission observed. Eu^{2+} forms a shallow trap below the conduction band and when electrons are excited, they are promoted to the conduction band and then trapped in the shallow traps [8] as depicted in **Figure 7**. The host material can also have intrinsic traps which can sometimes trap electrons [40]. These intrinsic traps are formed during the synthesis as gases escape. Ca^{2+} ions can be substituted by Eu^{2+} and Dy^{3+} ions because they have similar ionic radii. This substitution leads to the disruption of the charge balance causing the formation of cationic vacancies where electrons are captured to maintain the charge neutrality [9]. Introducing the Eu^{2+}ions as a dopant in the host material will lead to the formation of shallow traps below the conduction band where electrons can be trapped and re-trapped increasing the luminescence persistence. Adding Dy^{3+} as a co-dopant will lead to the formation of intermediate traps and deeper traps which can capture more electrons and hence lead to a longer afterglow of the phosphor.

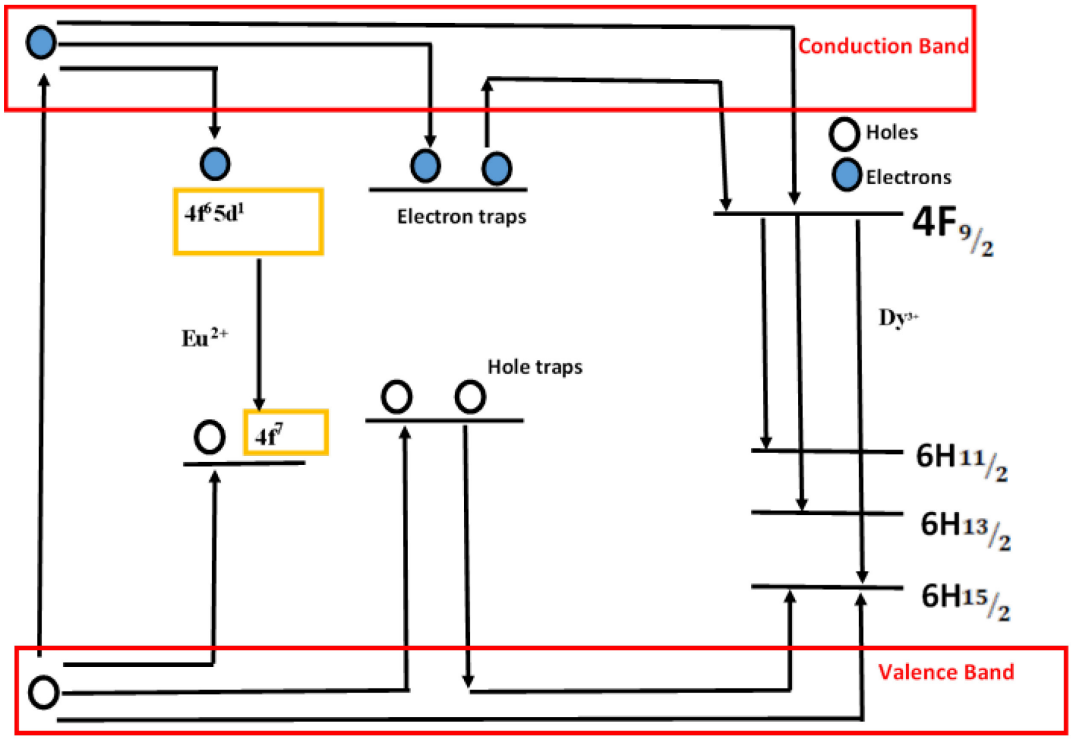

Figure 7 A schematic representation of PL mechanism in Eu^{2+}doped and Dy^{3+}co-doped $CaAl_2O_4$ phosphor.

Conclusions

The synthesis of $CaAl_2O_4$: Eu^{2+}, Dy^{3+} phosphor using the combustion method was successfully conducted, and the structural and optical properties of the samples synthesized at varying pH levels were analyzed using FTIR, XRD and UV-V is spectroscopy. Scanning electron microscopy was also employed to examine the morphology of the samples. The study shows that $CaAl_2O_4$: Eu^{2+}, Dy^{3+} phosphor synthesized at pH of 4.5 gave optimum synthesis pH producing the most crystalline sample for use in lighting devices. By meticulously controlling the pH levels during synthesis, researchers can finely tune the crystalline structure and luminescent properties of these nanoparticles. This precision enables optimization of their performance in optoelectronic devices, including light-emitting diodes and displays, by tailoring emission characteristics such as color purity and brightness. Furthermore, the ability to modulate pH facilitates the enhancement of luminescence efficiency, thus rendering these phosphors promising candidates for applications in biomedical imaging, security features and energy technologies. This study underscores the pivotal role of synthesis conditions, particularly pH, in dictating the properties of phosphors, exemplified by $CaAl_2O_4$: Eu^{2+}, Dy^{3+} nanoparticles. By systematically varying the pH during synthesis, researchers demonstrated pronounced alterations in the structural and optical characteristics of the resulting nanoparticles. This observation highlights the sensitivity of phosphor properties to subtle changes in synthesis parameters, underscoring the importance of precise control over synthesis conditions to tailor the properties of phosphors for specific applications.

References

[1] AH Wako, FB Dejene and HC Swart. Roles of doping ions in afterglow properties of blue $CaAl_2O_4$: Eu^{2+}, Nd^{3+} phosphors. *Phys. B Condens. Matter* 2014; **439**, 153-9.

[2] AH Wako, FB Dejene and HC Swart. Influence of alkaline earth metal cations; Ca^{2+}, Sr^{2+} and Ba^{2+} on the structural and optical properties of MAl_2O_4: Eu^{2+}, Nd^{3+} phosphors. *J. Dep. Phys. Sci.* 2014;

[3] X Han, J Han, C Liu and J Sun. Promise and challenge of phosphorus in science, technology, and application. *Adv. Funct. Mater.* 2018; **28**, 1803471.

[4] M Hoheisel. Review of medical imaging with emphasis on X-ray detectors. *Nucl. Instrum. Methods Phys. Res. Sect. A* 2006; **563**, 215-24.

[5] AH Wako, FB Dejene and HC Swart. Structural and luminescence properties of $SrAl_2O_4$: Eu^{2+}, Dy^{3+}, Nd^{3+} phosphor thin films grown by pulsed laser deposition. *Phys. B* 2016; **480**, 116-24.

[6] WM Yen and H Yamamoto. *Practical applications of phosphors.* CRC Press, Boca Raton, United States, 2018.

[7] D Haranath, P Sharma, H Chander, A Ali, N Bhalla and SK Halder. Role of boric acid in synthesis and tailoring the properties of calcium aluminate phosphor. *Mater. Chem. Phys.* 2007; **101**, 163-9.

[8] XL Yan, YX Liu, DT Yan, HC Zhu, CG Liu and CS Xu. The effects of Mn^{2+} doping on the luminescence properties of $12CaO{\cdot}7Al_2O_3$: Eu^{2+} nanocrystal phosphor. *J. Nanosci. Nanotechnol.* 2011; **11**, 9964-9.

[9] DC Rodriguez Burbano, SK Sharma, P Dorenbos, B Viana and JA Capobianco. Persistent and photostimulated red emission in CaS: Eu^{2+}, Dy^{3+} nanophosphors. *Adv. Opt. Mater.* 2015; **3**, 551-7.

[10] V Singh, V Natarajan and JJ Zhu. Luminescence and EPR investigations of Mn activated calcium aluminate prepared via combustion method. *Opt. Mater.* 2007; **30**, 468-72.

[11] AH Wako, FB Dejene and HC Swart. Combustion synthesis, characterization and luminescence properties of barium aluminate phosphor. *J. Rare Earths* 2014; **32**, 806-11.

[12] AH Wako. 2011, Preparation and properties of long afterglow $CaAl_2O_4$ phosphors activated by rare earth metal ions. Master Thesis. University of the Free State, Bloemfontein, South Africa.

[13] D Bokov, AT Jalil, S Chupradit, W Suksatan, MJ Ansari, IH Shewael, GH Valiev and E Kianfar. Nanomaterial by sol-gel method: synthesis and application. *Adv. Mater. Sci. Eng.* 2021; **2021**, 5102014.

[14] H Ryu, BK Singh, KS Bartwal, MG Brik and IV Kityk. Novel efficient phosphors on the base of Mg and Zn co-doped $SrTiO_3$: Pr^{3+}. *Acta Mater.* 2008; **56**, 358-63.

[15] YU Yuan, W Jian, W Jidong, LI Jing, ZHU Yanan, LI Ziaoqiang, SONG Xiaolei and GE Mingqiao. Structural characterization and optical properties of long-lasting $CaAl_2O_4$: Eu^{2+}, Nd^{3+} phosphors synthesized by microwave-assisted chemical co-precipitation. *J. Rare Earths* 2017; **35**, 652-7.

[16] M Zahedi, SA Hassanzadeh-Tabrizi and A Saffar-Teluri. Sol-gel synthesis and luminescence properties of Ba_2SiO_4: Sm^{3+} nanostructured phosphors. *Ceram. Int.* 2018; **44**, 10169-74.

[17] Y Chu, Q Zhang, Y Li, Z Liu, J Xu, H Zeng and H Wang. Hydrothermal synthesis of $Bi_4Ge_3O_{12}$: Eu^{3+} phosphors with high thermal stability and enhanced photoluminescence property. *J. Alloys Compd.* 2017; **693**, 308-14.

[18] X Huang, Q Sun and B Devakumar. Facile low-temperature solid-state synthesis of efficient blue-emitting $Cs_3Cu_2I_5$ powder phosphors for solid-state lighting. *Mater. Today Chem.* 2020; **17**, 100288.

[19] E Shafia, M Bodaghi, S Esposito and A Aghaei. A critical role of pH in the combustion synthesis of nano-sized $SrAl_2O_4$: Eu^{2+}, Dy^{3+} phosphor. *Ceram. Int.* 2014; **40**, 4697-706.

[20] CH Hsu and CH Lu. A critical role of pH in the combustion synthesis of nano-sized $SrAl_2O_4$: Eu^{2+}, Dy^{3+} phosphor. *Adv. Appl. Ceram.* 2009; **108**, 149-54.

[21] A Kumar, MHM Couto, SP Tiwari, K Kumar and JCG Esteves da Silva. Effect of pH of precursor on up/downconversion and cathodoluminescence of Gd_2O_3: Ho^{3+}/Yb^{3+} phosphor and magneto-optic studies. *Chemistryselect* 2018; **3**, 10566-73.

[22] AH Wako, FB Dejene and HC Swart. Combustion synthesis, characterization and luminescence properties of barium aluminate phosphor. *J. Rare Earths* 2014; **32**, 806-11.

[23] S Ekambaram, KC Patil and M Maaza. Synthesis of lamp phosphors: Facile combustion approach. *J. Alloys Compd.* 2005; **393**, 81-92.

[24] S Yang, G Xiao and D Ding. Characterization and separation resistance of an in-situ 2D nanocarbon/calcium aluminate composite synthesized via a combustion method. *J. Asian Ceram. Soc.* 2021; **9**, 1038-45.

[25] FB Dejene, MO Onani, LF Koao, AH Wako, SV Motloung and MT Yihunie. Structure, morphology and optical properties of undoped and MN-doped $ZnO_{(1-x)}S_x$ nano-powders prepared by precipitation method. *Phys. B Condens. Matter* 2016; **480**, 63-7.

[26] IP Sahu, DP Bisen, N Brahme, RK Tamrakar and R Shrivastava. Luminescence studies of dysprosium doped strontium aluminate white light emitting phosphor by combustion route. *J. Mater. Sci. Mater. Electron.* 2015; **26**, 8824-39.

[27] E Karacaoğlu. Synthesis and characterization of $CaAl_2O_4$: Dy^{3+} and $CaAl_2O_4$: Sm^{3+} phosphor powders. *El-Cezeri* 2022; **9**, 360-70.

[28] E Shafia, M Bodaghi, S Esposito and A Aghaei. A critical role of pH in the combustion synthesis of nano-sized $SrAl_2O_4$: Eu^{2+}, Dy^{3+} phosphor. *Ceram. Int.* 2014; **40**, 4697-706.

[29] CH Hsu and CH Lu. Influence of pH on the formation and luminescence properties of the sol-gel derived $SrAl_2O_4$: Eu^{2+}, Dy^{3+} phosphors. *Adv. Appl. Ceram.* 2009; **108**, 149-54.

[30] JP Rex, AA Nathan and M Vitalis. Crystal size effect on the photoluminescence of calcium aluminate doped Mn^{2+} nanocrystals. *Int. J. Phys. Sci.* 2015; **10**, 537-42.

[31] CC Lin and RS Liu. Advances in phosphors for light-emitting diodes. *J. Phys. Chem. Lett.* 2011; **2**, 1268-77.

[32] P Makuła, M Pacia and W Macyk. How to correctly determine the band gap energy of modified semiconductor photocatalysts based on UV-Vis spectra. *J. Phys. Chem. Lett.* 2018; **9**, 6814-7.

[33] N Sangiorgi, L Aversa, R Tatti, R Verucchi and A Sanson. Spectrophotometric method for optical band gap and electronic transitions determination of semiconductor materials. *Opt. Mater.* 2017; **64**, 18-25.

[34] REM Khaidir, YW Fen, MHM Zaid, KA Matori, NAS Omar, MF Anuar, SAA Wahab and AZK Azman. Exploring Eu^{3+}-doped ZnO-SiO_2 glass derived by recycling renewable source of waste rice husk for white-LEDs application. *Results Phys.* 2019; **15**, 102596.

[35] BP Kumara, KH Shivaprasada, RS Raveendrab, RH Krishnac and BM Nagabhushanac. Adsorption of hazardous methylene blue from aqueous solution using combustion derived $CaAl_2O_4$ nanoparticles. *J. Mater. Sci. Surf. Eng.* 2016; **4**, 492-5.

[36] MM Colen. 2015, Synthesis and characterization of long persistent phosphors using combustion method. Master Thesis. University of South Africa, Pretoria, South Africa.

[37] E Shafia, M Bodaghi, S Esposito and A Aghaei. A critical role of pH in the combustion synthesis of nano-sized $SrAl_2O_4$: Eu^{2+}, Dy^{3+} phosphor. *Ceram. Int.* 2014; **40**, 4697-706.

[38] C Rosticher, B Viana, G Laurent, P le Griel and C Chanéac. Insight into $CaMgSi_2O_6$: Eu^{2+}, Mn^{2+}, Dy^{3+} nanoprobes: Influence of chemical composition and crystallinity on persistent red luminescence. *Eur. J. Inorg. Chem.* 2015; **2015**, 3681-7.

[39] F Xue, Y Hu, L Fan, G Ju, Y Lv and Y Li. Cr^{3+}-activated $Li_5Zn_8Al_5Ge_9O_{36}$: A near-infrared long-afterglow phosphor. *J. Am. Ceram. Soc.* 2017; **100**, 3070-9.